ELSEVIER

Microelectronics Journal 34 (2003) 815–821

Microelectronics Journal

www.elsevier.com/locate/mejo

# Efficient inductance calculation in interconnect structures by applying the Monte Carlo method

Christian Harlander*, Rainer Sabelka, Siegfried Selberherr

*Institute for Microelectronics, TU Vienna, Gusshausstr. 27-29/E360, A-1040 Vienna, Austria*

Received 29 October 2002; revised 3 March 2003; accepted 7 April 2003

**Abstract**

We present an advanced algorithm for an extraction tool to compute inductances of interconnect structures. As already pointed out [Proc. Third Int. Conf. Modeling Simul. Microsyst. (2000) 416] the pursued energy concept leads to a 6-fold integral which can also be evaluated by use of the Monte Carlo method. A classical implementation of the Monte Carlo method, where the whole geometry has to be hunted for an associated element loses efficiency. Our approach is applied without time consuming element location for the random point coordinates to compute this integral. The precalculated current density distribution is computed with the finite element method. Geometrical modeling is done with an unstructured tetrahedral mesh to gain high flexibility and to ensure a latter integration of the process flow. Hence, some simplifications compared to the real geometry, as other published approaches usually do implicitly, are not required.


*Keywords:* Finite element method; Interconnect analysis; Inductance; Monte Carlo method

## 1. Introduction

Conventional circuit design techniques were focused primarily on minimizing the chip size. Thus the influence of the interconnect structures cannot be neglected anymore, aspects as signal delay, inductive and capacitive crosstalk, attenuation of the signal and reliability are becoming important issues. Because of increasing operating frequencies and the usage of new materials like copper and low-κ dielectrics, inductive effects gain significance especially for lines, which provide power supply or global busses. A necessary, but not sufficient condition for consideration of inductive effects is that the impedance of the inductive part is of the same order of magnitude as the resistance of the line. In addition, several inequalities describe the area, where inductive effects are not negligible and have to be considered in the design [2].

A suitable choice of the aspect ratio (thickness/width) improves RC delay. Maximum benefits are achieved at an aspect ratio of ~2 [3]. To include clock frequency in the design of multilevel networks, the longest local and semi-global interconnects on each tier have a time delay less than 25% of the clock period. The remaining 75% clock cycle is dedicated to the time delay of the critical paths and clock skew. A hierarchical approach is given in Ref. [4]. The calculation of crosstalk is usually performed with closed formulae for certain cases (parallel lines above ground, parallel lines between two levels) [5]. Efficient crosstalk calculation is performed by an extended model to include inductive effects [6]. For long global lines the time delay is decreased by the insertion of inverters. The signal shape is improved at the expense of the package density and the energy consumption. Information about the arrangement of inverters is given [7]. Global routing techniques and shielding are required to minimize the inductive crosstalk, which can involve also far distant lines [8]. Shielding features are utilized combined with order reduction method to gain area efficient solution under the constraint of crosstalk [9].

The calculation of inductive effects needs the concept of partial inductances [10], because a priori the current path is not completely known. Beside lengthy analytic formulations, as e.g. for rectangular conductors [11], better suited formulae for computational evaluation of long, thin lines are given in Ref. [12]. A closed formula with 16 evaluations of one function for rectangular conductors provides [13]. Through segmentation the skin effect can be modeled inside

* Corresponding author. Fax: +43-1-58801-36099.
*E-mail address:* harlander@iue.tuwien.ac.at (C. Harlander).

0026-2692/03/$ - see front matter © 2003 Elsevier Science Ltd. All rights reserved.
doi:10.1016/S0026-2692(03)00147-2

the conductors. Based on the network theory, not the current density distribution is explicitly calculated, but the current density distribution is approximated with small filaments carrying a certain current with a constant current density. From filament to filament the current density varies, hence a step function approximation of the actual current density is obtained. Solving the current loop equations of the partial equivalent element circuits the divergenceless magnetic vector potential is fulfilled. The conceived partial equivalent element circuits tends to large, sparsely occupied matrices, hence a model order reduction treatment may be necessary.

Beside FastHenry [14] other simulators [15], are based on approximation formulae from Grover [16] or other relevant formulae to obtain partial inductances for simple geometries. The latter one is restricted to stratified geometries and conductors with rectangular cross-section, which can also be exploited to calculate capacitances using a Green function approach.

## 2. The program package

The calculation of the current density distribution is performed with the Smart Analysis Programs [17]. Therefore, we use the finite element method, because of advantages, as numerical robustness, the ability to solve nonlinear systems, high obtained accuracy, and general applicability. Fig. 1 gives an overview about the Smart Analysis Programs.

The geometry can be defined either directly from the layout by specifying layer thicknesses, or by a rigorous topography simulation [18,19]. So the inductance extraction is in principle not limited to idealized Manhattan-like geometries as in the approaches presented in the introduction. The layout of the interconnect structure can also be imported from CIF or GDSII files, or created interactively with a graphical layout editor [20]. Furthermore, the program package includes three preprocessors, one for two-dimensional applications (CUTGRID) the other for three-dimensional applications. The preprocessor LAYGRID allows a layer-based input of the simulation geometry and the specification of the boundary conditions on the borders of each subdomain. The fully unstructured three-dimensional Delaunay grid generator DELINK [21] utilize an advanced-front algorithm, whereby the mesh generation starts from an initial front to fill up the solids with tetrahedrons.

A preconditioned conjugate gradient solver (ICCG), which has been optimized specifically for the discretized Laplace operator, is used to solve the linear systems for domains of conducting materials [22]. By applying Ohm's law to the derivative of the electrostatic potential the distribution of the electric current density is obtained. The simulation is performed with the module STAP (Smart Thermal Analysis Program), where both inductance extraction methods have been implemented.

Two postprocessors complete the program package, whereby the visualization tool SV is based on VTK [23], a flexible and powerful visualization library. Both postprocessors can be used to verify the grid quality, and for the visualization of several distributions (e.g. electric potential, temperature, current density), whereby SV provides numerous features, as e.g. cutting plains, volume rendering and contour faces representation of distributions.

## 3. Physical approach

We compare two stationary inductance calculation methods both based on a numerical solution of Neumann's formula [16] for a precalculated current density distribution:

$$L_{ik} = \frac{\mu}{4\pi}\frac{1}{I_i I_k}\int_{V_i}\int_{V_k'}\frac{\mathbf{J}_i(\mathbf{r})\cdot\mathbf{J}_k(\mathbf{r}')}{|\mathbf{r}-\mathbf{r}'|}\,\mathrm{d}V\,\mathrm{d}V'. \tag{1}$$

The integration is carried out numerically, where special attention has to be paid on the singularities of the integrand, or with the Monte Carlo method. For both methods the stationary current density is calculated with the finite element method. The first method [1] employs a summation of the contributions of all pairs of finite elements to solve the integral (1), where different kinds of approximation are used, depending on the term $|\mathbf{r}-\mathbf{r}'|$. For a large distance (compared to the tetrahedron diameter) simple integration formulae are sufficient. The evaluation for small distances demands special formulae with certain integration points, published by Stroud [24] who presented various integration formulae which are applicable for $n$-simplexes (e.g. the unit triangle, the unit tetrahedron) as integration region. If $\mathbf{r}$ and $\mathbf{r}'$ are in the same tetrahedron, a partially analytic integration scheme is used to increase the accuracy of the integration.

## 4. The Monte Carlo method

A well-known choice for the evaluation of multiple integrals is to apply the Monte Carlo method. Associated with this method, where by random the point coordinates are chosen, is a fairly high demand on CPU-time, because of the time consuming search for the associated element of the random point coordinates. To reduce the error a high number of function evaluations has to be carried out, whereby for each evaluation the aligned element with the precalculated current density must be found. To improve the convergence during the Monte Carlo sampling several variance reduction schemes (e.g. importance sampling, control variates) are known to accelerate the computation procedure [25].

### *4.1. Implementation*

One big advantage of our implementation is to bypass the high computational effort for the element location. We first

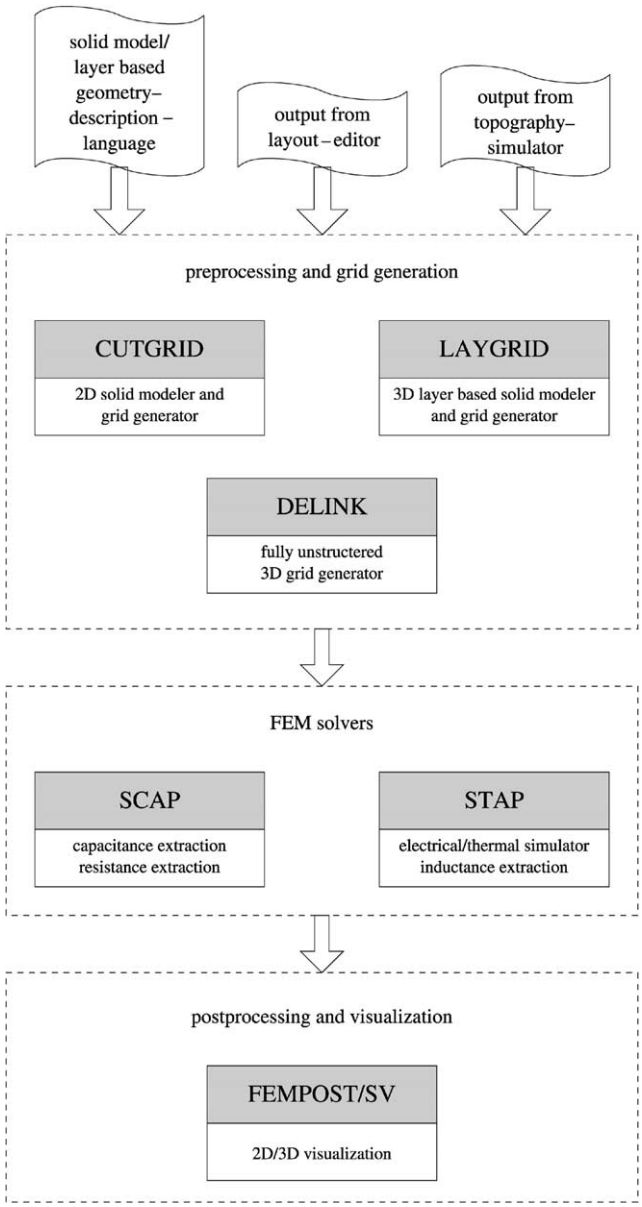


Fig. 1. The Smart Analysis Programs: tools and dataflow.

determine the associated element to the evaluated probability function, and then locate the point inside the tetrahedron. For this purpose we take two arrays for every conductive segment. The first one holds the volume of each element, whereby the sum of all entries is scaled to one. The second one stores the probability function already evaluated for each conductor element by adding up all entries from the beginning to the current index of the first array. Then the random generator chooses a number between zero and one. The associated element complying to the probability function is found by a binary search. The procedure is pictured in Fig. 2. To ensure a uniform probability the local coordinates of the integration points are found by shooting into the unit cube. The first point inside the registered unit tetrahedron is taken. For the interpolation of the current density inside each element quadratic shape functions are used.

### *4.2. Application example*

Figs. 3 and 4 show the current density of two planar transformers. These transformers are built of two interwound spirals each of 3, respectively, 5-turns metal with 5 μm width, a spacing of 15 μm, and an inner length of 54 μm.

By utilizing the preprocessor LAYGRID three different grids were made. In Table 1 the simulation times for the current density and the Monte Carlo method, respectively,

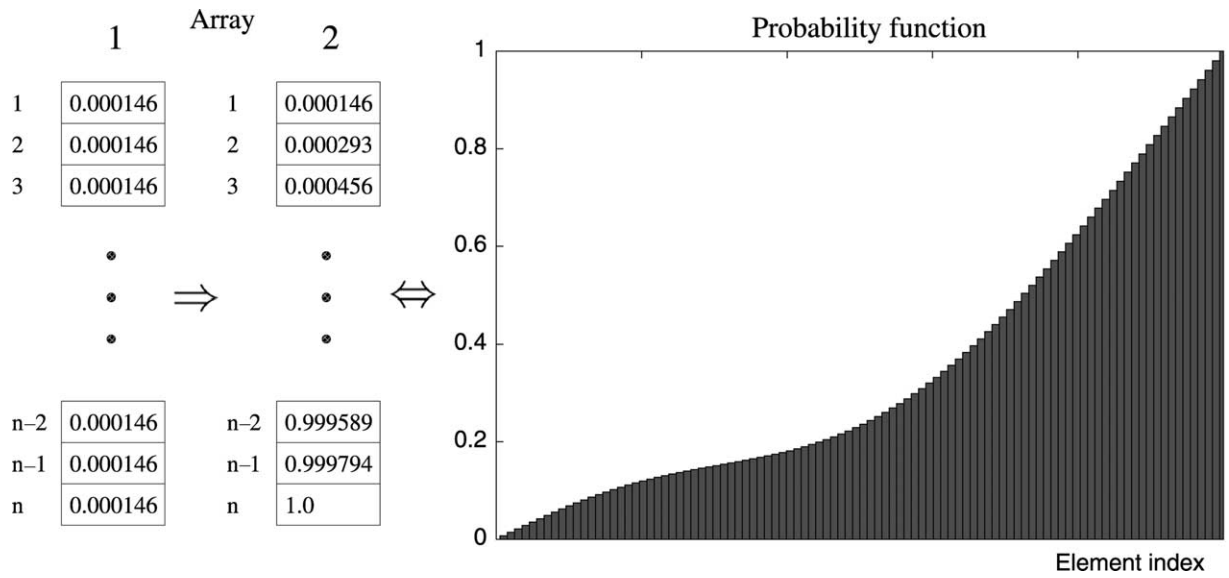


Fig. 2. Illustration of the element determination.

the first numeric method as accomplished above, and the calculated inductances are listed. The simulations were performed on a Digital Alpha workstation (DEC600/333 MHz). The minimum number of samples for the Monte Carlo method was 1 million. This gives due to the Monte Carlo error estimation for the 99.99% confidence interval the mutual inductance with $\pm 0.9\%$ and the self inductance with $\pm 1.8\%$ in Table 1 according to Eq. (3). The first column of Table 1 implies all elements of the conductive segments, whereby tetrahedral grid elements with quadratic shape functions were used. The analysis time for the Monte Carlo method is not so strongly influenced by the number of elements ($n$), because the computational effort for the binary search grows with $\ln(n)$. The simple integration formulae for the mutual inductances demand almost the same time with increasing $n$. Table 1 emphasizes the advantage of the Monte Carlo method explicitly.

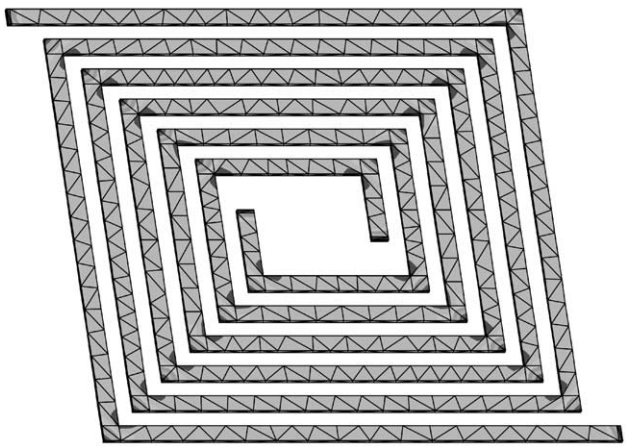

Fig. 3. Current density distribution of the planar transformer with 3-turns metal.

### 4.3. Convergence, estimation of the simulation error

Figs. 5 and 6 give details about the convergence behavior for the calculation of the self and mutual inductance. Both curves show explicitly the continuous decrease of the fluctuation margin, in Fig. 5 quicker than in Fig. 6. For the mutual inductance the variance is smaller, therefore, fewer samples suffice to reach the same accuracy as for the self inductance, due to the term $|\mathbf{r} - \mathbf{r}'|$ in the denominator. The evaluation of the mutual inductance is characterized by a larger distance between the evaluation points, thereby the integrand fluctuates not in the extent as for the self inductance. Errors sources are in the evaluation of Eq. (1) and the computation of the current density. These independent error sources can be handled separately. In order to minimize the influence of

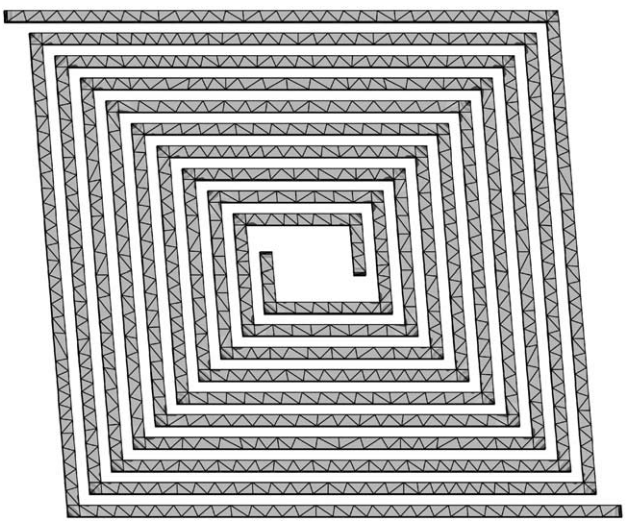

Fig. 4. Current density distribution of the planar transformer with 5-turns metal.

Table 1
Analysis time and results of the planar transformers: M and L stand for mutual and self inductance, respectively, and MC refers to the Monte Carlo method

| Number of elements | Time (s) | | | | Results (nH) | | | |
|---|---|---|---|---|---|---|---|---|
| | MC | | Method [1] | | MC | | Method [1] | |
| | M | L | M | L | M | L | M | L |
| *3-turns* | | | | | | | | |
| 1800 | 17 | 33 | 1 | 327 | 0.67 | 1.04 | 0.67 | 1.06 |
| 1968 | 17 | 34 | 1 | 627 | 0.67 | 1.05 | 0.67 | 1.06 |
| 2648 | 18 | 34 | 3 | 1764 | 0.67 | 1.06 | 0.67 | 1.06 |
| *5-turns* | | | | | | | | |
| 4383 | 18 | 35 | 7 | 1945 | 2.71 | 3.58 | 2.70 | 3.62 |
| 4653 | 19 | 35 | 8 | 2088 | 2.71 | 3.60 | 2.70 | 3.62 |
| 5697 | 19 | 36 | 15 | 7885 | 2.70 | 3.60 | 2.69 | 3.63 |

inaccuracies from the current density, techniques for mesh refinements can be applied. Corresponding to the resulting changes of the calculated inductances only a differential—not an absolute—error can be specified (except a comparison with analytic solutions).

The error estimation within the Monte Carlo method is feasible without big effort according the Eqs. (2) and (3), thereby the specification for the abort criteria of the procedure is possible. The Monte Carlo algorithm terminates, if the fluctuation of the results is below a given level. The error $\Delta L_{ik}$ can be calculated with the variance $\sigma_{ik}^2$ of the samples $L_{ik_\tau}$

$$\sigma_{ik}^2 = \frac{1}{N}\sum_{\tau} L_{ik_\tau}^2 - \left(\frac{1}{N}\sum_{\tau} L_{ik_\tau}\right)^2 \tag{2}$$

and the number of samples $N$ (99.99% confidence interval)

$$\Delta L_{ik} = 3\frac{\sigma_{ik}}{\sqrt{N}}. \tag{3}$$

The Monte Carlo method with the abort criteria needs only a continuous computation of the standard deviation from Eq. (3) with Eq. (2). If $\Delta L_{ik}/L_{ik} < \epsilon$ is fulfilled, the algorithm is terminated. The error bounds of the estimation value decreases with $1/\sqrt{N}$. To reduce the limit by a factor $c$, the required number of samples (and effort) increases with $c^2$.

### 4.4. Influence of the singularities

The integrand in Eq. (4) is singular for $\mathbf{r} = \mathbf{r}'$. To investigate the influence of the singularity the integral is separated in two integrals over the same region, $I_1$ and $I_2$,

$$I = I_1 + I_2 = \int_V \mathrm{d}V \int_V \mathrm{d}V' \frac{\mathbf{J}(\mathbf{r})\cdot\mathbf{J}(\mathbf{r}')}{|\mathbf{r}-\mathbf{r}'|}. \tag{4}$$

The first integral excludes the singularity

$$I_1 = \int\int_{|\mathbf{r}-\mathbf{r}'|>\delta} \mathrm{d}V\,\mathrm{d}V' \frac{\mathbf{J}(\mathbf{r})\cdot\mathbf{J}(\mathbf{r}')}{|\mathbf{r}-\mathbf{r}'|} \tag{5}$$

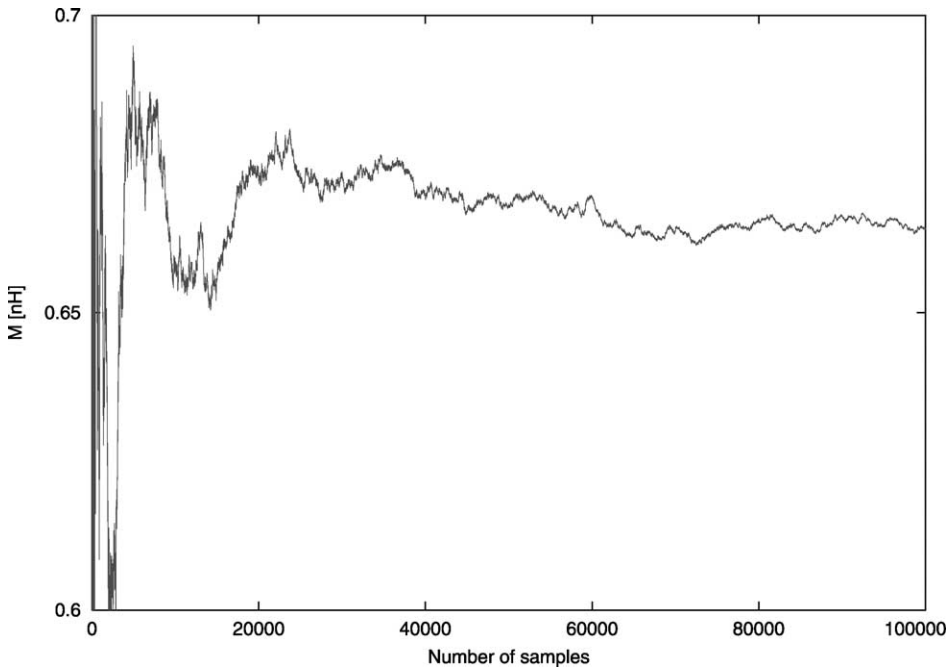


Fig. 5. Convergence diagram for the computation of the mutual inductance over the first 10% of the minimum number of samples (transformer with three windings).

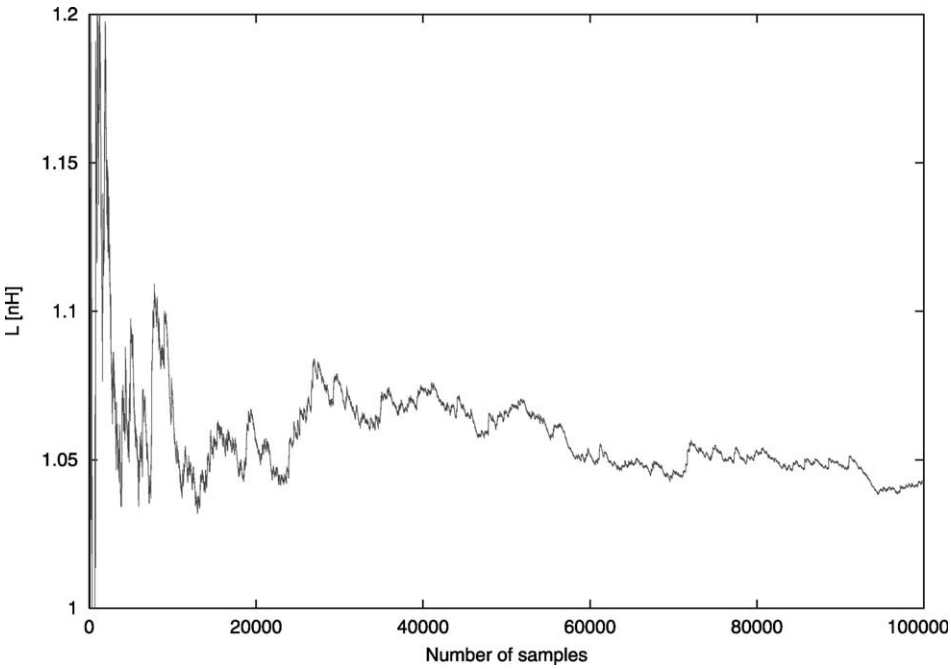


Fig. 6. Convergence diagram for the computation of the self inductance over the first 10% of the minimum number of samples (transformer with three windings).

and is evaluated as before. The region for the second integral is a small sphere around the singularity

$$I_2 = \int\int_{|\mathbf{r}-\mathbf{r}'|<\delta} \mathrm{d}V\,\mathrm{d}V' \frac{\mathbf{J}(\mathbf{r})\cdot\mathbf{J}(\mathbf{r}')}{|\mathbf{r}-\mathbf{r}'|}. \tag{6}$$

Because of the small distance $\mathbf{r}-\mathbf{r}'$ the current density $\mathbf{J}(\mathbf{r}')$ can be enveloped linearly about $\mathbf{r}$

$$\mathbf{J}(\mathbf{r}') \approx \mathbf{J}(\mathbf{r}) + \nabla\mathbf{J}(\mathbf{r})\cdot(\mathbf{r}-\mathbf{r}'). \tag{7}$$

Set in $I_2$ results

$$I_2 = \int_V \mathrm{d}V \mathbf{J}(\mathbf{r})\cdot\mathbf{J}(\mathbf{r}) \overbrace{\int_{|\mathbf{r}-\mathbf{r}'|<\delta} \mathrm{d}V' \frac{1}{|\mathbf{r}-\mathbf{r}'|}}^{I_{21}} + \int_V \mathrm{d}V \mathbf{J}(\mathbf{r})\nabla\mathbf{J}(\mathbf{r}) \overbrace{\int_{|\mathbf{r}-\mathbf{r}'|<\delta} \mathrm{d}V' \frac{\mathbf{r}-\mathbf{r}'}{|\mathbf{r}-\mathbf{r}'|}}^{I_{22}}, \tag{8}$$

$$I_{21} = \int_{|\mathbf{r}-\mathbf{r}'|<\delta} \mathrm{d}V' \frac{1}{|\mathbf{r}-\mathbf{r}'|} = \int_0^\delta \frac{4\pi R^2}{R}\mathrm{d}R = 2\pi\delta^2. \tag{9}$$

The integral $I_{22}$ vanishes due to symmetry reasons

$$I_{22} = \int_0^\delta \int_0^{2\pi} \int_0^\pi R^2 \sin\vartheta\,\mathrm{d}\vartheta\,\mathrm{d}\varphi\,\mathrm{d}R \frac{1}{R} \begin{pmatrix} R\sin\vartheta\cos\varphi \\ R\sin\vartheta\sin\varphi \\ R\cos\vartheta \end{pmatrix} = 0. \tag{10}$$

With the representation

$$I = \int\int_{|\mathbf{r}-\mathbf{r}'|>\delta} \mathrm{d}V\,\mathrm{d}V' \frac{\mathbf{J}(\mathbf{r})\cdot\mathbf{J}(\mathbf{r}')}{|\mathbf{r}-\mathbf{r}'|} + \int_V \mathrm{d}V \mathbf{J}(\mathbf{r})\cdot\mathbf{J}(\mathbf{r})\cdot 2\pi\delta^2 \tag{11}$$

a sensitivity analysis is possible, to work out the influence of the parameter $\delta$. On the basis of a simple demonstration example this is realized (Fig. 7). The cross-section of the geometric loop amounts $1\times 1\ \mu\mathrm{m}^2$. The whole loop can be wrapped into a box with $9\times9\times3\ \mu\mathrm{m}^3$. The evaluation from Eq. (11) shows that with increasing reduction of $\delta$ the contribution from the second term disappears. A typical magnitude of $\delta=2\mathrm{nm}$ for the geometric loop, below no contribution is yielded from the second term. For $|\mathbf{r}-\mathbf{r}'|<2\mathrm{nm}$ this term can be neglected. $\delta$ is not a constant factor. It depends on the actual example. As reference value for the geometric

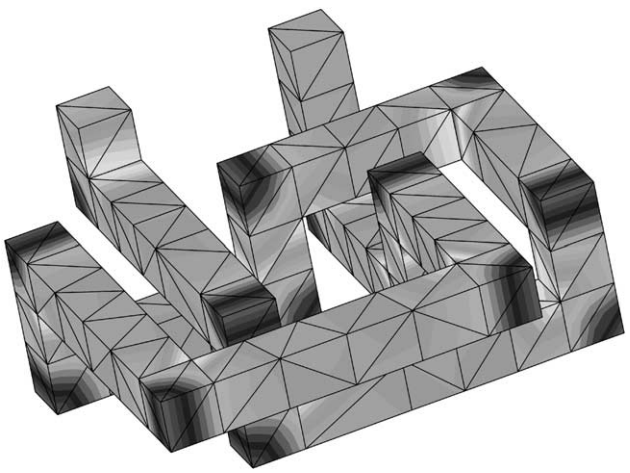

Fig. 7. Current density distribution of the geometrical loop.

loop can be stated that $\delta$ is about 2% of the shortest edge length of a typical tetrahedron. Hence it is shown that for $\delta \to 0$ the formulation Eq. (11) is equivalent to the original one. The Monte Carlo method is not influenced by the singularity, because the probability to evaluate the integrand there is zero.

## 5. Conclusion

An advanced Monte Carlo algorithm for effective inductance calculation in interconnect structures has been presented. The presented approach is not limited to idealized geometries of interconnect structures. We have compared two numerical techniques for the computation of inductances. Both methods are implemented into the package Smart Analysis Programs, which allows simultaneous extraction of three-dimensional effective parameters of VLSI circuits.

## Acknowledgements

This work has been supported by the European Community MULSIC project IST-2000-30133.

## References

[1] C. Harlander, R. Sabelka, S. Selberherr, Inductance calculation in interconnect structures, Proceedings of the Third International Conference on Modeling and Simulation of Microsystems, San Diego, CA, USA, 2000, pp. 416–419.

[2] A. Deutsch, G.V. Kopcsay, P.J. Restle, H.H. Smith, G. Katopis, W.D. Becker, P.W. Coteus, C.W. Surovic, B.J. Rubin, J.D.R.P.T. Gallo, K.A. Jenkins, L.M. Terman, R.H. Dennard, G.A. Sai-Halasz, B.L. Krauter, D.R. Knebel, When are transmission-line effects important for on-chip interconnections?, IEEE Transactions on Microwave Theory and Techniques 45 (10) (1997) 1836–1846.

[3] M. Bohr, Interconnect scaling—the real limiter to high performance ULSI, Proceedings of the International Electronic Devices Meeting, 1995, pp. 241–244.

[4] H. Su, S. Sapatnekar, Hybrid structured clock network construction, Proceedings of the IEEE/ACM International Conference on Computer-Aided Design, San Jose, USA, 2001, pp. 333–336.

[5] J. Rey, J. Li, V. Boksha, D. Adalsteinsson, J. Sethian, Topography simulation for interconnect deposition, Solid State Technology 2 (1998) 77–82.

[6] M. Kuhlmann, S. Sapatnekar, Exact and efficient crosstalk estimation, IEEE Transactions on Computer-Aided Design of Integrated Circuits and Systems 20 (7) (2001) 858–866.

[7] C.J. Alpert, J. Hu, S.S. Sapatnekar, P.G. Villarrubia, A practical methodology for early buffer and wire resource allocation, Proceedings of the Design Automation Conference'01, 38th Design Automation Conference, Las Vegas, USA, 2001, pp. 189–193.

[8] Y. Massoud, S. Majors, T. Bustami, J. White, Layout techniques for minimizing on-chip interconnect self inductance, Proceedings of the Design Automation Conference'98, ACM, San Francisco, USA, 1998, pp. 566–571.

[9] J.D.Z. Ma, L. He, Formulae and applications of interconnect estimation considering shield insertion and net ordering, Proceedings of the IEEE/ACM International Conference on Computer-Aided Design, San Jose, USA, 2001, pp. 327–332.

[10] E.B. Rosa, The self and mutual inductances of linear conductors, Bulletin of the Bureau of Standards 4 (2) (1907) 301–344.

[11] C. Hoer, C. Love, Exact inductance equations for rectangular conductors with applications to more complicated geometries, Journal of Research of the National Bureau of Standards 69C (2) (1965) 127–137.

[12] A.E. Ruehli, Inductance calculations in a complex integrated circuit environment, IBM Journal of Research and Development 16 (5) (1972) 470–481.

[13] W.T. Weeks, L.L. Wu, M.F. McAllister, A. Singh, Resistive and inductive skin effect in rectangular conductors, IBM Journal of Research and Development 23 (6) (1979) 652–660.

[14] M. Kamon, M.J. Tsuk, J. White, FastHenry: a multipole accelerated 3-D inductance extraction program, IEEE Transactions on Microwave Theory and Techniques 42 (9) (1994) 1750–1758.

[15] A.M. Niknejad, R.G. Meyer, Analysis and optimization of monolithic inductors and transformers for RF ICs, Proceedings of the IEEE Custom Integrated Circuits Conference, 1997, pp. 375–378.

[16] F.W. Grover, Inductance Calculations: Working Formulas and Tables, D. Van Nostrand Company, New York, 1946.

[17] R. Sabelka, S. Selberherr, A finite element simulator for three-dimensional analysis of interconnect structures, Microelectronics Journal 32 (2) (2001) 163–171.

[18] W. Pyka, R. Martins, S. Selberherr, Optimized algorithms for three-dimensional cellular topography simulation, IEEE Journal of Technology Computer Aided Design 2000 http://www.ieee.org/products/online/journal/tcad/accepted/Pyka-March00/

[19] R. Martins, W. Pyka, R. Sabelka, S. Selberherr, Modeling integrated circuit interconnections, Proceedings of the International Conference on Microelectronics and Packaging, Curitiba, Brazil, 1998, pp. 144–151.

[20] R. Martins, S. Selberherr, Layout data in TCAD frameworks, Modelling and Simulation, Society for Computer Simulation International, 1996.

[21] P. Fleischmann, W. Pyka, S. Selberherr, Mesh generation for application in technology CAD, IEICE Transactions on Electronics E82-C (6) (1999) 937–947.

[22] R. Bauer, S. Selberherr, Preconditioned CG-solvers and finite element grids, Proceedings of the CCIM, Breckenridge, USA, vol. 2, 1994.

[23] W. Schroeder, K. Martin, B. Lorensen, The Visualization Toolkit: an Object-Oriented Approach to 3D Graphics, Prentice-Hall, Englewood Cliffs, NJ, 1996.

[24] A.H. Stroud, Approximate Calculation of Multiple Integrals, Prentice-Hall, Englewood Cliffs, NJ, 1971.

[25] G. Leonhardt, W. Fichtner, Acceleration of inductance extraction by means of the Monte Carlo method, Technical Report 99/8, Integrated Systems Laboratory, ETH Zürich, 1999.